In Situ Synthesis of A_3-Type Star Polymer/Clay Nanocomposites by Atom Transfer Radical Polymerization

Muhammed Aydin,[1] Mehmet Atilla Tasdelen,[1,2] Tamer Uyar,[3] Yusuf Yagci[1,4]

[1]Department of Chemistry, Faculty of Science and Letters, Istanbul Technical University, Maslak, TR-34469 Istanbul, Turkey
[2]Department of Polymer Engineering, Faculty of Engineering, Yalova University, TR-77100 Yalova, Turkey
[3]UNAM-Institute of Materials Science and Nanotechnology, Bilkent University, TR-06800 Ankara, Turkey
[4]King Abdulaziz University, Center of Excellence for Advanced Materials Research (CEAMR) and Chemistry Department, Faculty of Science, P. O. Box 80203, , Jeddah, 21589 Saudi Arabia
Correspondence to: M. A. Tasdelen (E-mail: tasdelen@yalova.edu.tr) or Y. Yagci (E-mail: yusuf@itu.edu.tr)

Received 21 June 2013; accepted 16 September 2013; published online 11 October 2013
DOI: 10.1002/pola.26957

ABSTRACT: A series of A_3-type star poly(methylmethacrylate)/clay nanocomposites is prepared by *in situ* atom transfer radical polymerization (ATRP) initiated from organomodified montmorillonite containing quaternary trifunctional ATRP initiator. The first order kinetic plot shows a linear behavior, indicating the controlled character of the polymerization. The resulting nanocomposites are characterized by spectroscopic (XRD), thermal (DSC and TGA), and microscopic (TEM) analyses. The exfoliated nanocomposite has been obtained when polymerization was conducted with 1% of organic clay loading. Thermal analyses show that all nanocomposites have higher glass transition values and thermal stabilities compared to neat polymer. © 2013 Wiley Periodicals, Inc. J. Polym. Sci., Part A: Polym. Chem. **2013**, *51*, 5257–5262

KEYWORDS: atom transfer radical polymerization; *in situ* polymerization; nanoclay; nanocomposites; star polymers

INTRODUCTION Through the combination of organic and inorganic compounds in one single material at nanoscopic level is one of the most effective approaches for producing new materials with advanced properties that were usually unavailable in the past.[1] These hybrid materials are easily available due to unique availability of the inorganic nanofillers such as, clays, carbon nanotubes, graphites, polyhedral oligomeric silsesquioxane (POSS), and metal oxides.[2] Among the various nanometric fillers, silicate-based clays are preferred being indeed the best candidates for their superior mechanical, thermal, and, most important, optical properties.[3] Several synthetic approaches namely, solution exfoliation, melt intercalation, *in situ* polymerization, and template synthesis, have been used for the preparation of polymer/clay nanocomposites.[4] The *in situ* polymerization is widely used method to prepare polymer/clay nanocomposites because of the types of nanofillers and polymer precursors can be varied in a wide range to get the enhanced properties.[5] In this method monomer, initiator, and/or catalyst are intercalated into silicate layers and the *in situ* polymerization is initiated by externally stimulation such as thermal, photochemical, or chemical activation. The growth of polymer chains within the clay galleries not only triggers to the exfoliation of the layered silicate in the polymer matrix but also results the formation of polymer/clay nanocomposites. The main challenge in nanocomposite synthesis is to develop reliable and versatile methods that ensure and maintain the random dispersion of the single silicate layers and, simultaneously, provide more control over the polymer architecture, such as functionality, composition, and dimensions. These well-defined structures also increase the interaction between the polymer matrix and the silicate layers and thereby increase the probability of forming exfoliated nanocomposites. The best way to achieve such a control is by using living and controlled/living polymerization methods.[6,7] Although most of the efforts have been concentrated on homopolymer-based nanocomposites,[8–22] there is also interest in nanocomposites containing complexes macromolecular architectures because of their structural and technological significance.[23] However, there are few reports on *in situ* preparation of nanocomposites containing block,[24–29] graft copolymers,[30,31] and hyperbranched polymers.[32–35] Star polymers exhibit different properties from those of their linear counterparts, such as such as less entanglement in the solid state, high solubility in various solvents, low melt viscosity, and fast molecular motion. Previously, Singh et al.

Additional Supporting Information may be found in the online version of this article.

used a self-consistent field theory to investigate the interactions between clay layers and star-shaped polymers.[36] It was reported that the relatively compact size of the star polymer combined with the surface of the clay promotes the miscibility of the nanocomposites. Later on, this behavior was proved experimentally by Robello et al. who prepared star polymer/montmorillonite nanocomposites by melt blending technique using star-shaped polystyrene with five arms ($M_n = 37{,}100$, PDI = 1.25) and organically modified MMT (Cloisite 10A or 15A).[37]

In this work, we synthesized a quaternary tri-functional atom transfer radical polymerization (ATRP) initiator, which can be directly intercalated into the silicate layers by ion exchange reaction. *In situ* ATRP of methyl methacrylate (MMA) leads to A_3-type star polymer/MMT nanocomposites possessing partially exfoliated/intercalated nanolayers in the polymer matrix.

EXPERIMENTAL

Materials

Sodium montmorillonite (Cloisite Na^+; Na-MMT) was purchased from Southern Clay products with cation exchange capacity (CEC) of 92.6 mequiv/100 g used as received. MMA (99%, Aldrich) was passed through a basic alumina column to remove the inhibitor. *N*,*N*,*N*′,*N*″,*N*″-pentamethyldiethylenetriamine (PMDETA, 99%, Aldrich) as a ligand, was distilled before use. Triethanolamine (98%, Aldrich), triethylamine (99%, Aldrich), 1-bromooctadecane (97%, Aldrich), copper(I) bromide (97%, Aldrich), and 2-bromoisobutyryl bromide (98%, Aldrich) were used as received. Other solvents were purified by conventional drying and distillation procedures.

Synthesis of Trifunctional ATRP Initiator

Triethanolamine (5.0 g, 33.5 mmol) and triethylamine (60 mL) were added to 200 mL dry THF. 2-Bromoisobutyryl bromide (24.7 mL, 45.98 g, 0.2 mol) was added dropwise to this mixture over 1 h at 0 °C. After stirring for a further 2 h, the triethylammonium hydrochloride salt was removed by filtration, and the resulting clear solution was concentrated under vacuum at 30 °C before washing with 0.1 M Na_2CO_3. The product was extracted three times with dichloromethane and the combined organic extract was dried with magnesium sulfate. Removal of the solvent under vacuum afforded a dark-reddish brown oil (18 g, yield: 90%).[38]

Synthesis of Quaternary Trifunctional ATRP Initiator

The initiator (8.9 g; 15 mmol) solved in 30 mL dry ethanol, 1-bromooctadecane (6.7 mL, 30 mmol) was added, and the mixture was stirred 2 days at 70 °C. After evaporation, the residue was recrystallized in the mixture of acetone and ethanol three times. Then, it was dried *in vacuo* at ambient temperature for 24 h (9.3 g; yield: 60%).

IR (ATR, cm^{-1}): 3650, 3400, 2930, 2850, 1660, 1470, 1400, 1120, 1000, 910, 790, 720, 605. ^1H NMR (D_2O): 1.20–1.35(37H), 1.80–1.90(18H), 2.55–2.65(6H), 3.35–3.45(6H) ppm. ^{13}C NMR (D_2O): 8.5(—**C**H_3), 22.3(—**C**H_2—), 25.9 (—**C**H_2—), 29.5 (—**C**H_2—), 33.5 (**C**H_3—C—Br), 51.5 (CH_3—**C**—Br), 59.5 (—O—**C**H_2—CH_2—N), 63.0 (—CH_2—**C**H_2—N), 64.5 (—O—CH_2—**C**H_2—N), 171.1 (—**C**=O) ppm.

Preparation of Organically Modified Clay

The organically modified montmorillonite (O-MMT) containing trifunctional ATRP initiator was prepared through cationic exchange between sodium montmorillonite (Na-MMT) and quaternary trifunctional ATRP (Q-tris-ATRP) initiator in an aqueous solution. A separate solution of MMT (1 g) and Q-tris-ATRP initiator (0.5 g, 0.6 mmol) was dispersed in 50 mL of deionized water at 50 °C for 24 h. Then, the two solutions were mixed vigorously and the total volume was brought up to 100 mL and stirred for 48 h at 50 °C. After mixing, the T-MMT was recovered by filtering the solution, followed by repeated washings of the filter cake with deionized water to remove the excess of ions. The final product was dried in a vacuum oven at room temperature for 24 h.

Synthesis of A_3-Type Star Polymer/Clay Nanocomposites

The organophilic clay (O-MMT, 1, 3, 6, and 10% of the monomer by weight), monomer (MMA, 130 mmol, 1.872 g), ligand (PMDETA, $9.6.10^{-3}$ mmol, 2 μL) and copper(I) bromide (Cu^IBr, $9.6.10^{-3}$ mmol, 1.4 mg), and toluene (2 mL as solvent) were mixed into a round bottom flask. The reaction mixture was degassed by three freeze-pump-thaw cycles and left in vacuum. The mixture was placed in a thermostated oil bath at 90 °C for 16 h. At the end of the polymerization, the mixture was precipitated into methanol, filtered, dried, and weighted.

Characterization

Molecular weights were determined by gel permeation chromatography (GPC) using an instrument consisting of a Viscotek GPCmax Autosampler, a pump, three ViscoGEL GPC columns ($G2000H_{HR}$, $G3000H_{HR}$, and $G4000H_{HR}$), and a Viscotek differential refractive index (RI) detector with a THF flow rate of 1.0 mL min^{-1} at 30 °C. The RI detector was calibrated with polystyrene standards having narrow molecular weight distribution. Data were analyzed using Viscotek OmniSEC Omni–01 software. Before the GPC measurement, the polymer was cleaved from clay by LiBr refluxing in tetrahydrofuran for about 24 h, followed by centrifugation and filtration through a filter. The powder X-ray diffraction (XRD) measurements were performed on a PANalytical X'Pert PRO X-ray diffractometer equipped with graphite-monochromatized Cu K_α radiation ($\lambda = 1.15$ Å). Differential scanning calorimetry (DSC) was performed on a Perkin-Elmer Diamond DSC with a heating rate of 20 °C min^{-1} under nitrogen flow (20 mL min^{-1}). Thermogravimetric analysis (TGA) was performed on a Perkin-Elmer Diamond TA/TGA with a heating rate of 10 °C min^{-1} under nitrogen flow (200 mL min^{-1}). Transmission electron microscopy (TEM) imaging of the samples was carried out on a FEI Tecnai™ G^2 F30 instrument operating at an acceleration voltage of 200 kV. Ultrathin TEM specimens (ca. 100 nm) were prepared by using a cryo-ultramicrotome ($EMUC_6 + EMFC_6$, Leica) equipped with a diamond knife. The ultrathin samples were placed on holey carbon-coated grids for TEM analyses.

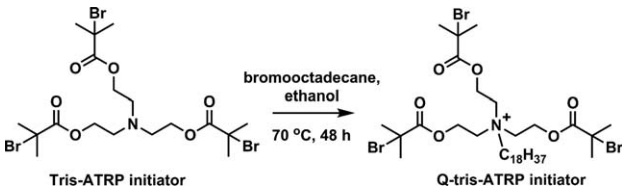

SCHEME 1 Synthesis of quaternized trifunctional ATRP initiator (Q-tris-ATRP initiator).

RESULTS AND DISCUSSION

Star polymers are essentially prepared either by the "arm-first" method, where preformed polymer chains are linked to the central core or the "core-first" method, where polymer chains are grown from a multifunctional core initiator. Because of a variety of controlled/living polymerization methods and their accompanying choice of monomers, the core-first method is a versatile and efficient synthetic strategy, and it has been widely used. Our synthetic strategy is based on designing a core molecule possessing both intercalation and multifunctional initiator functionalities to be used for ATRP of MMA. This was done in a two-step procedure; (i) esterification reaction between 2-bromopropionyl bromide and triethanolamine, and (ii) quaternization of trifunctional ATRP initiator with 1-bromooctadecane (Scheme 1). The structure of the resulting quaternized trifunctional ATRP initiator (Q-tris-ATRP initiator) was confirmed by spectral analysis (See Supporting Information Figs. S1 and S2).

The successful incorporation of Q-tris-ATRP initiator into the clay surface was confirmed by FTIR, XRD, and TGA analyses. The characteristic peaks at 1740 and 1005 cm^{-1} are attributed to C═O and Si—O group of the Q-tris-ATRP initiator and clay in the FTIR spectrum (See Supporting Information Fig. S2). On the other hand, the diffraction peak was shifted to a lower angle after ion exchange, indicating an increase of the interlayer distance of the clay sheets of 0.4 nm for the organophilic clay (O-MMT). This change indicated that the Q-tris-ATRP initiator was successfully intercalated into the silicate galleries of the MMT clay. The thermal gravimetric analysis (TGA) was performed to calculate the organic content of O-MMT after modification. The mass losses were 7.1 and 20.1% for sodium-montmorillonite (Na-MMT) and O-MMT, respectively corresponding to 13% attachment of Q-tris-ATRP initiator (See Supporting Information Fig. S3).

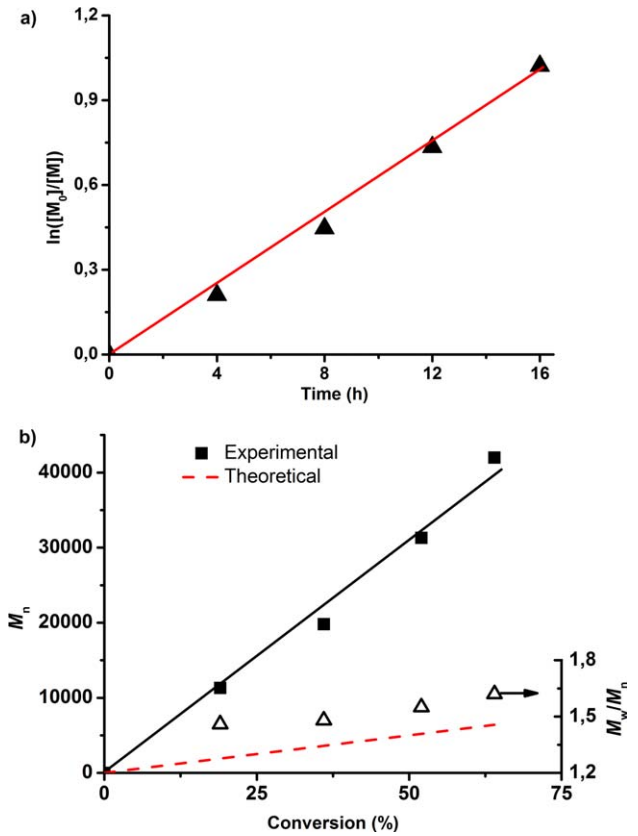

FIGURE 1 ATRP of methyl methacrylate ($[MMA]_0/[R\text{-}X]_0/[Cu^IBr]_0/[L]_0 = 100/1/3/3$), (a) kinetic plot and (b) molecular weights and distributions of resulting polymers as a function of degree of conversion. [Color figure can be viewed in the online issue, which is available at wileyonlinelibrary.com.]

ATRP of MMA was carried out at 90 °C in bulk, using O-MMT as multifunctional ATRP initiator and Cu^IBr as catalyst in combination with PMDETA as ligand. The kinetic plot and the evolution of molecular weight and distribution with conversion for the ATRP targeting DP = 100 were investigated. The monomer consumption ($\ln([M]_0/[M])$) versus the polymerization time plots was linear, which indicated that the propagating radical concentrations were almost constant during the polymerization (Fig. 1). The molecular weights increased linearly with conversions, which were consistent with the polymerizations proceeding in a controlled fashion.

TABLE 1 ATRP of Methyl Methacrylate in the Presence of Different Amount Organophilic Clay[a]

Run	*O*-MMT (wt %)	[MMA]/[R-X]/[L]/[Cu^IBr]	Conv.[b] (%)	$M_{n,GPC}$[d] (g mol^{-1})	$M_{n,GPC}$[d] (g mol^{-1})	M_w/M_n[d]
NC-0	0	100/1/3/3	78	7,900	17,000	1.48
NC-1	1	100/1/3/3	62	6,400	42,000	1.62
NC-3	3	50/1/3/3	77	4,200	28,000	1.67
NC-6	6	50/1/3/3	86	4,100	23,000	1.45
NC-10	10	30/1/3/3	91	3,000	19,000	1.53

[a] Polymerization reaction was carried out in bulk at 90 °C for 16 h.
[b] Determined by gravimetrically.
[c] $M_{n,Th} = [MMA]_0/([R\text{-}X]_0 \times M_{W,MMA} \times Cnv.$
[d] Molecular weight and distribution were determined by gel permeation chromatography.

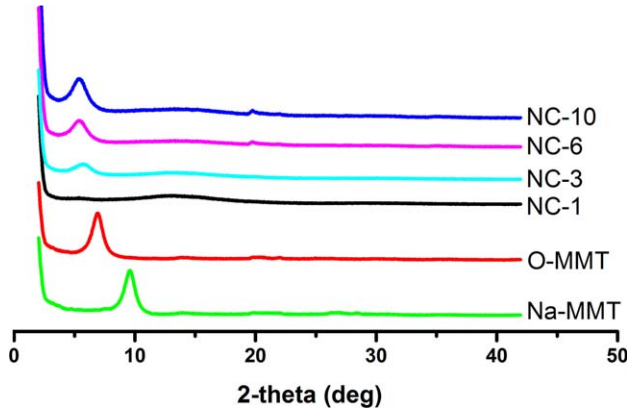

FIGURE 2 X-ray diffractions of Na-MMT, O-MMT, and obtained nanocomposites (NC-1, 3, 6, and 10). [Color figure can be viewed in the online issue, which is available at wileyonlinelibrary.com.]

The molecular weight distribution remained narrow (1.45–1.62) and unimodal during the polymerization. However, the experimental molecular weights were much higher than the theoretical values, indicating low initiation efficiency. This might be due to the restricted mobility of Q-tris-ATRP initiator tethered nanoclay platelets.

Table 1 summarizes the results of ATRP of MMA in the presence of different amount of nanoclay. The polymer obtained in the absence of nanoclay (Table 1, NC-0) had molecular weight value close to the theoretical one and relatively narrow molecular weight distribution (1.48). Compared to the heterogeneous system, it showed better control of molecular weight and distribution under the same experimental conditions. With an increase in nanoclay initiator amount, there was an increase in polymerization rate, which results in the higher conversion of MMA polymerization and lower the molecular weights of the resulting polymers.

XRD diffractograms of Na-MMT (6.95°), O-MMT (6.82°), and PMMA/MMT nanocomposites at different clay loading are illustrated in Figure 2. The basal space (d_{001}) was expanded after the cation exchange with Q-tris-ATRP initiator from 1.28 to 1.31 nm. After the polymerization, this peak

FIGURE 3 TEM micrographs showing exfoliated/intercalated silicate layers in NC-1 (a), NC-3 (b), NC-6 (c), and NC-10 (d) samples at higher magnification (scale bar: 20 nm). [Color figure can be viewed in the online issue, which is available at wileyonlinelibrary.com.]

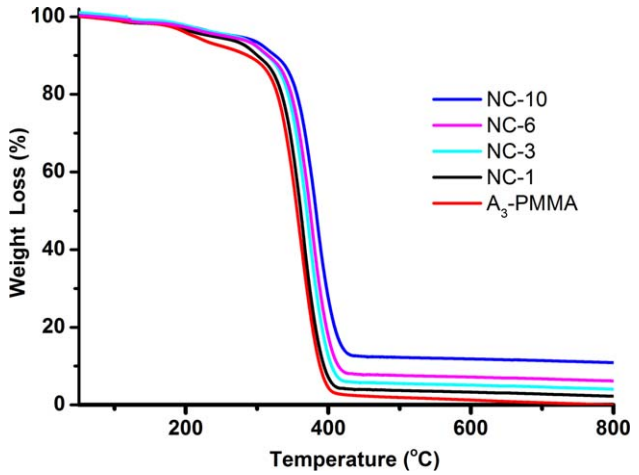

FIGURE 4 TGA thermograms of A_3-PMMA and PMMA/MMT nanocomposites (NC-1, 3, 6, and 10). [Color figure can be viewed in the online issue, which is available at wileyonlinelibrary.com.]

disappeared in the XRD pattern of NC-1 sample, which indicates the formation of exfoliated structure of clay. However, it was found that partially exfoliated or intercalated structures existed in the high clay content system (NC-3, 6, and 10) probably due to the difficulty for overcoming the intensive ionic attraction between the neighboring platelets.

Although XRD is a convenient and practical tool to determine intercalated and exfoliated morphologies, in certain cases its reliability is limited due to the clay dilution, preferred orientation, mixed layering, and other peak broadening factors. Direct imaging techniques such as atomic force microscopy (AFM), scanning electron microscopy (SEM), or TEM are often combined to strengthen the conclusion derived from XRD analysis. Figure 3 presents the high magnification TEM images of the nanocomposites containing 1, 3, 6, and 10 wt % O-MMT, respectively. The dark lines represent the silicate layers; about 1.0 nm thick and from 50 to 100 nm in lateral dimension, which are oriented perpendicularly to the slicing plane and the gray areas correspond to the polymer matrix. As the TEM images showed that the dispersion of clay exhibits different morphologies, including intercalated regions with a nonuniform separation of the layers and exfoliated single layers isolated from any stack. TEM analysis also confirmed that the degree of exfoliation in the nanocomposites decreased with increasing clay loading in the process. This might be due to the high loading degree or molecular weight of polymer matrix. The polymer with higher molecular weight (NC-1) is more beneficial for exfoliated structure than low molecular weight polymer (NC-3, 6, and 10). Combined together with the results of XRD and TEM, it could be concluded that the interlayer spacing derived from XRD is just an average value for a mixed morphology of intercalated and exfoliated clays, and not an actual value for a well-defined interlayer distance in regularly intercalated montmorillonites.

Thermal degradation behavior of neat A_3-PMMA star polymer and PMMA/MMT nanocomposites at various loading prepared via ATRP was studied by TGA, heating from room temperature to 800 °C under inert atmosphere. As indicated in Figure 4, the thermal behavior of the nanocomposite is quite similar to the neat polymer and single step decomposition was observed for all nanocomposite samples. It was found that the nanocomposites had much higher T_{onset} (temperature at 5% weight loss) and T_{max} (temperature at 50% weight loss) than the neat polymer (Table 2). This beneficial effect can be explained by addition of clay as an inorganic material with high thermal stability and great barrier properties that can prevent the heat from transmitting quickly and can limit the continuous decomposition. However, the thermal degradation temperatures of the nanocomposites with different organic clay loadings were very close to each other, and no significant trend with increasing clay content was observed. Notably, the final char yields of nanocomposites were increased with increase in weight percent of clay loading.

DSC analysis of neat A_3-PMMA star polymer and PMMA/MMT nanocomposites was carried out to determine glass transition temperature (T_g) values of the nanocomposites at

TABLE 2 Physical Properties of PMMA/MMT Nanocomposites and Their Components for Comparison

			Weight Loss Temperature[c] (°C)		
Entries	d_{001}[a] (nm)	Tg[b] (°C)	%10	%50	Char. Yield[c] (%)
Na-MMT	0.90	–	–	–	92.9
O-MMT	1.30	–	565	–	79.9
A_3-PMMA	–	123.1	286	348	<1
NC-1	–	130.8	300	361	2.3
NC-3	1.55	128.4	313	369	4.1
NC-6	1.60	128.3	316	374	6.4
NC-10	1.66	129.0	325	382	10.9

[a] Basal spacing (d_{001}) is calculated by XRD analysis.
[b] Determined by DSC and analyses under a nitrogen flow at a heating rate of 10 °C min^{-1}.
[c] Determined by TGA analysis under a nitrogen flow at a heating rate of 10 °C min^{-1}.

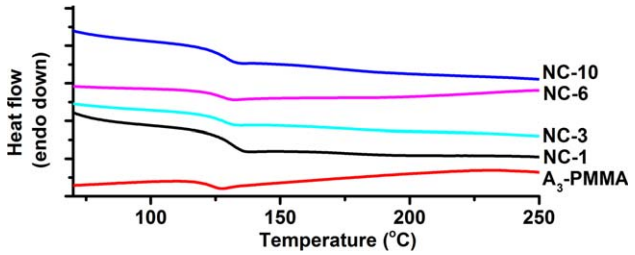

FIGURE 5 DSC traces of A_3-PMMA star polymer and PMMA/MMT nanocomposites (NC-1, 3, 6, and 10). [Color figure can be viewed in the online issue, which is available at wileyonlinelibrary.com.]

various clay loadings (Fig. 5). The T_g of polymers depends mainly on the molecular structure of the polymer (chain stiffness, number, architecture, and bulkiness of the side groups, and the intermolecular and intramolecular interactions) and on the crosslink density of the polymer. All nanocomposite samples had high T_g value than neat polymer. The highest value of NC-1 nanocomposite can be ascribed to its molecular weight and exfoliation morphology with fine dispersion of silicate layers in the polymer matrix that provides large surface area for clay interacting with polymer matrix, which can be lead to the restricted segmental motions near the organic–inorganic interfaces. Conclusively, there was no significant improvement of T_g of nanocomposites with the increase of the clay content.

CONCLUSIONS

The sodium montmorillonite was successfully functionalized with trifunctional ATRP initiator, which was confirmed by XRD, TGA and FTIR analyses. A series of A_3-PMMA star PMMA/MMT nanocomposites have been prepared by *in situ* ATRP of MMA. Linear kinetic plot and increase in molecular weight with conversion indicated that ATRP of MMA was controlled. Spectroscopic and microscopic investigations revealed a complex morphology, with partial intercalation/exfoliation, which depends on the concentration of clay. DSC and TGA analyses showed that all nanocomposites have higher T_g value and thermal stabilities compared to neat A_3-PMMA star polymer.

The exfoliated nanocomposite has been obtained when polymerization was conducted with 1% of organic clay loading. However, with increasing the clay loading to 3, 6, and 10%, the degree of exfoliation of the nanocomposites decreased, which confirmed by both XRD and TEM analyses. This may be due to short chain length of branches of the star polymer. From TGA, an improvement in the thermal stability of obtained nanocomposites was noted even at 1% of clay loading.

ACKNOWLEDGMENTS

M. Aydin and Y. Yagci thank Istanbul Technical University, Research Fund for financial support.

REFERENCES AND NOTES

1 C. Sanchez, G. Soler-Illia, F. Ribot, T. Lalot, C. R. Mayer, V. Cabuil, *Chem. Mater.* **2001**, *13*, 3061–3083.

2 A. C. Balazs, T. Emrick, T. P. Russell, *Science* **2006**, *314*, 1107–1110.

3 M. Alexandre, P. Dubois, *Mater. Sci. Eng. R* **2000**, *28*, 1–63.

4 S. S. Ray, M. Okamoto, *Prog. Polym. Sci.* **2003**, *28*, 1539–1641.

5 E. P. Giannelis, *Adv. Mater.* **1996**, *8*, 29–35.

6 M. A. Tasdelen, J. Kreutzer, Y. Yagci, *Macromol. Chem. Phys.* **2010**, *211*, 279–285.

7 H. Roghani-Mamaqani, V. Haddadi-Asl, M. Salami-Kalajahi, *Polym. Rev.* **2012**, *52*, 142–188.

8 M. Aydin, M. A. Tasdelen, T. Uyar, S. Jockusch, N. J. Turro, Y. Yagci, *J. Polym. Sci. Part A: Polym. Chem.* **2013**, *51*, 1024–1028.

9 C. Dizman, S. Ates, T. Uyar, M. A. Tasdelen, L. Torun, Y. Yagci, *Macromol. Mater. Eng.* **2011**, *296*, 1101–1106.

10 K. D. Demir, M. A. Tasdelen, T. Uyar, A. W. Kawaguchi, A. Sudo, T. Endo, Y. Yagci, *J. Polym. Sci. Part A: Polym. Chem.* **2011**, *49*, 4213–4220.

11 C. Altinkok, T. Uyar, M. A. Tasdelen, Y. Yagci, *J. Polym. Sci. Part A: Polym. Chem.* **2011**, *49*, 3658–3663.

12 A. Oral, M. A. Tasdelen, A. L. Demirel, Y. Yagci, *J. Polym. Sci. Part A: Polym. Chem.* **2009**, *47*, 5328–5335.

13 A. Oral, M. A. Tasdelen, A. L. Demirel, Y. Yagci, *Polymer* **2009**, *50*, 3905–3910.

14 M. A. Tasdelen, W. Van Camp, E. Goethals, P. Dubois, F. Du Prez, Y. Yagci, *Macromolecules* **2008**, *41*, 6035–6040.

15 H. Akat, M. A. Tasdelen, F. Du Prez, Y. Yagci, *Eur. Polym. J.* **2008**, *44*, 1949–1954.

16 A. Nese, S. Sen, M. A. Tasdelen, N. Nugay, Y. Yagci, *Macromol. Chem. Phys.* **2006**, *207*, 820–826.

17 M. A. Tasdelen, *Eur. Polym. J.* **2011**, *47*, 937–941.

18 M. Huskic, E. Zagar, M. Zigon, *Eur. Polym. J.* **2012**, *48*, 1555–1560.

19 M. Huskic, M. Zigon, *J. Appl. Polym. Sci.* **2009**, *113*, 1182–1187.

20 M. Huskic, M. Zigon, *Eur. Polym. J.* **2007**, *43*, 4891–4897.

21 H. Y. Zhao, S. D. Argoti, B. P. Farrell, D. A. Shipp, *J. Polym. Sci. Part A: Polym. Chem.* **2004**, *42*, 916–924.

22 H. Bottcher, M. L. Hallensleben, S. Nuss, H. Wurm, J. Bauer, P. Behrens, *J. Mater. Chem.* **2002**, *12*, 1351–1354.

23 M. A. Tasdelen, Y. Yagci, *Aust. J. Chem.* **2011**, *64*, 982–991.

24 Z. Yenice, M. A. Tasdelen, A. Oral, C. Guler, Y. Yagci, *J. Polym. Sci. Part A: Polym. Chem.* **2009**, *47*, 2190–2197.

25 H. Y. Zhao, B. P. Farrell, D. A. Shipp, *Polymer* **2004**, *45*, 4473–4481.

26 J. Di, D. Y. Sogah, *Macromolecules* **2006**, *39*, 5052–5057.

27 N. K. Singha, A. Kavitha, D. J. Haloi, P. Mandal, A. Janke, D. Jehnichen, H. Komber, B. Voit, *Macromol. Chem. Phys.* **2012**, *213*, 2034–2043.

28 D. J. Haloi, S. Ata, N. K. Singha, *Ind. Eng. Chem. Res.* **2012**, *51*, 9760–9768.

29 H. Y. Zhao, D. A. Shipp, *Chem. Mater.* **2003**, *15*, 2693–2695.

30 W. J. Bae, K. H. Kim, W. H. Jo, Y. H. Park, *Macromolecules* **2004**, *37*, 9850–9854.

31 J.-M. Raquez, Y. Nabar, R. Narayan, P. Dubois, *J. Appl. Polym. Sci.* **2011**, *122*, 639–647.

32 P. K. Maji, P. K. Guchhait, A. K. Bhowmick, *ACS Appl. Mater. Interfaces* **2009**, *1*, 289–300.

33 H. Deka, N. Karak, *Nanoscale Res. Lett.* **2009**, *4*, 758–765.

34 H. Deka, N. Karak, *Polym. Adv. Technol.* **2011**, *22*, 973–980.

35 H. Deka, N. Karak, *Mater. Chem. Phys.* **2010**, *124*, 120–128.

36 C. Singh, A. C. Balazs, *Polym. Int.* **2000**, *49*, 469–471.

37 D. R. Robello, N. Yamaguchi, T. Blanton, C. Barnes, *J. Am. Chem. Soc.* **2004**, *126*, 8118–8119.

38 Y. T. Li, R. Narain, Y. H. Ma, A. L. Lewis, S. P. Armes, *Chem. Commun.* **2004**, 2746–2747.